

Article

# Proposing Wavelet-Based Low-Pass Filter and Input Filter to Improve Transient Response of Grid-Connected Photovoltaic Systems

Bijan Rahmani and Weixing Li \*

Department of Electrical Engineering, Harbin Institute of Technology, Harbin 150001, China;  
bijanrahmanix@gmail.com

\* Correspondence: wxli@hit.edu.cn; Tel.: +86-158-0451-8519

Academic Editor: Tapas Mallick

Received: 3 June 2016; Accepted: 10 August 2016; Published: 18 August 2016

**Abstract:** Available photovoltaic (PV) systems show a prolonged transient response, when integrated into the power grid via active filters. On one hand, the conventional low-pass filter, employed within the integrated PV system, works with a large delay, particularly in the presence of system's low-order harmonics. On the other hand, the switching of the DC (direct current)–DC converters within PV units also prolongs the transient response of an integrated system, injecting harmonics and distortion through the PV-end current. This paper initially develops a wavelet-based low-pass filter to improve the transient response of the interconnected PV systems to grid lines. Further, a damped input filter is proposed within the PV system to address the raised converter's switching issue. Finally, Matlab/Simulink simulations validate the effectiveness of the proposed wavelet-based low-pass filter and damped input filter within an integrated PV system.

**Keywords:** photovoltaic (PV) system; wavelet-based low-pass filter; damped input filter; transient response

## 1. Introduction

Rapid growth of non-linear loads increases the presence of harmonics in power systems. These harmonics lead to the false operation of circuit breakers and relays, reduction in transmission system efficiency, malfunction of electronic equipment, and overheating of transformers. Thus, active filters are introduced within power systems to address the issue. Further, the active filters are also employed to integrate the renewable distributed sources, like photovoltaic (PV) units to power systems [1]. Nonetheless, the available active filters work inaccurately, since the employed second-order low-pass filter within their compensation algorithms (namely advanced generalized theory of instantaneous power (A-GTIP) algorithm [2], synchronous reference frame d-q-r algorithm [3], and the p-q-based method) works with a large delay [4]. Accordingly, the active filter's reaction time also worsens the transient response of an integrated PV unit to the power system. Meanwhile, when the grid-end current contains low-order harmonics, the conventional second-order low-pass filter is unable to fully separate the positive-sequence component of grid-end active power [5]. This additionally results in the malfunction of employed active filter. Furthermore, the injection of generated PV power to AC grid will be prolonged due to the large delay of the second-order low-pass filter. To address these issues, this paper develops a wavelet-based low-pass filter, using the second generation wavelet theory [6–10]. Then, the wavelet-based low-pass filter is applied to an advanced universal power quality conditioning system (AUPQS) ([2] for the AUPQS active filter). The improved AUPQS is able to fully suppress power system harmonics and distortions in a less transient response time. Further, the developed lifting-based wavelet filter is also applied to extract the positive sequence of generated PV power.

On the other hand, the integrated PV system-to-AC grid usually involves one DC–DC converter, employed to track the maximum power point of the PV system [11–19]. However, this DC–DC converter’s switching itself prolonged the PV unit’s response time, leading the PV system to include pulsating current harmonics [20–24].

In [25–27], new topologies were suggested for high-order power filters for single-phase grid-tied voltage source inverters. These suggestions are the same, as this paper focused on compensating the harmonics and distortions generated through grid-tied inverters. This paper, moreover, considers and improves the transient response of the grid-tied photovoltaic (PV) system by accurately selecting the proposed input filter’s elements.

Here, the input filter is proposed to eliminate the DC–DC converter switching effect on PV systems. However, if not designed well, the input filter would change the dynamics of the integrated PV system, inserting two unstable complex poles into the system transfer function. This results in the PV system working unstably. Hence, this paper introduces an optimized damped input filter as a solution, addressing the issue, while providing higher electrical efficiency to the integrated PV system.

This paper initially briefly analyzes the lifting-based wavelet theory to develop a wavelet-based low-pass filter. Further, the wavelet-based low-pass filter is employed through the AUPQS controller to extract the positive sequence components of both the grid-end active power and the generated PV power. Accordingly, the transient response of an integrated PV unit to the power system using the AUPQS is discussed. Furthermore, a damped input filter is designed to eliminate the DC–DC converter’s switching effect within the integrated PV system, and the principles and criteria needed to be taken into account for damping the designed input filter are presented. Finally, Matlab/Simulink Software (MathWorks, Miami, FL, USA) is employed to verify the effectiveness of the proposed wavelet-based low-pass filter, as well as the accuracy of the suggested damped input filter within an integrated PV system to the power supply.

## 2. Practical Issues and Proposed Solutions

As shown in Figure 1, two solutions exist to improve the transient response of an integrated PV/grid system. The first is to employ a wavelet-based low-pass filter instead of the conventional low-pass filters within both the AUPQS and PV unit. The second is to use a damped input filter within the PV’s DC–DC converter to shorten the transient response. These solutions are investigated here through two subsections.

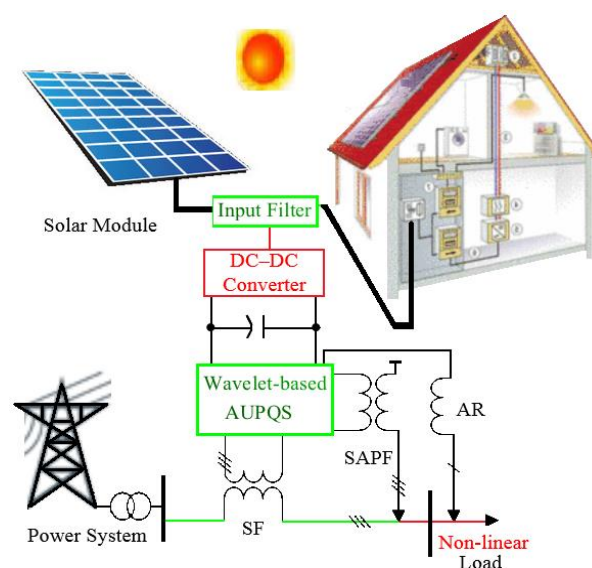


**Figure 1.** The proposed wavelet-based advanced universal power quality conditioning system (AUPQS) and the input filter within an integrated photovoltaic (PV) system.

## 2.1. The Wavelet-Based Low-Pass Filter

### 2.1.1. Lifting-Based Wavelet Theory

Wavelet transform approximates the power signals based on their involved correlation in time and frequency. The conventional wavelet transform, based on the Fourier series, translates/dilates a few basic shapes to build the time–frequency localization of a signal [28,29]. However, this wavelet transform method cannot perfectly reconstruct every signal, since its reverse transform includes rounding errors within the floating point operation. Moreover, in the traditional wavelet method, the original signal cannot be replaced with its wavelet transform. So, the extra auxiliary memory is always needed. Thus, the second-generation wavelet transform, based on the lifting scheme, is introduced in the spatial domain. The lifting method does not depend on Fourier transforms, i.e., translation/dilation of one specific function. It also does not involve complex mathematical calculations, so that a full in-place calculation becomes possible. Now the question is do the lifting schemes always exist for every traditional wavelet transform. As shown in [5–10], the lifting scheme always exists for a wavelet transform as long as the determinant of its poly-phase matrix equals one. This means that the pair of high-pass and low-pass finite impulse response (FIR) filters was complementary. The lifting–based wavelet transforms comprise following steps. First step is to split the data into odd and even sets. Then, low-frequency signals would be “updated” within the prime lifting step and the high–frequency signals are so called “predicted” within the dual lifting step.

#### (A) Splitting step

Different methods can be used to split a signal into two parts, such as directly cutting of the sampled sequence into left and right sets. However, in that case, the sampled signal in each part may not be well-correlated. In other words, predicting of one set using the other set is not an easy job. Another method is to classify the data sequence based on the odd and even frames as it is shown in Equation (1).

In traditional multi-resolution wavelet method, the odd/even splitting step is assumed at the end of each decomposition step using down–sampling. This means low and high-pass filters’ coefficients are first calculated, and then half of them throw away inefficiently. However, the second-generation wavelet method initially interlaces the sampled signal into odd/even datasets (Equation (1)), and then the low-frequency and high–frequency signals are evaluated as follows through both update and predict steps:

$$\left\{ \begin{array}{l} \begin{bmatrix} LP(z^2) \\ HP(z^2) \end{bmatrix} = \frac{1}{2} \begin{bmatrix} \tilde{h}(-z) & \tilde{h}(z) \\ \tilde{g}(-z) & \tilde{g}(z) \end{bmatrix} \begin{bmatrix} f(-z) \\ f(z) \end{bmatrix} \\ \begin{bmatrix} \tilde{\lambda}(z) \\ \tilde{\gamma}(z) \end{bmatrix} = \underbrace{\begin{bmatrix} \tilde{h}_e(z) & \tilde{h}_o(z) \\ \tilde{g}_e(z) & \tilde{g}_o(z) \end{bmatrix}}_{\tilde{P}(z): \text{ polyphase matrix}} \begin{bmatrix} f_e(z) \\ z^{-1}f_o(z) \end{bmatrix} \end{array} \right. \quad (1)$$

where  $\tilde{h}(z)$  and  $\tilde{g}(z)$  are low-pass and high-pass FIR filters, which are determined based on a mother wavelet, “e” and “o” denote the even and odd sequences, respectively.  $\tilde{\lambda}(z)$  contains the low-frequency signal coefficients and  $\tilde{\gamma}(z)$  includes the high-frequency signal coefficients.

#### (B) Update/predict steps

Updating leads the low frequency sub-signals involved in the original signal to remain unchanged, and the predict step extracts the high frequency sub-signals of the original signal, subtracting the odd

datasets from the even sets. It is worth noting that several lifting schemes are possible for a specific mother wavelet. Two common lifting schemes are as follows:

$$\left\{ \begin{array}{l} \left\{ \begin{array}{l} P(z) = \prod_{i=1}^m \begin{bmatrix} 1 & S_i(z) \\ 0 & 1 \end{bmatrix} \begin{bmatrix} 1 & 0 \\ t_i(z) & 1 \end{bmatrix} \begin{bmatrix} K & 0 \\ 0 & 1/K \end{bmatrix} \\ \tilde{P}(z) = \prod_{i=1}^m \begin{bmatrix} 1 & 0 \\ -S_i(z^{-1}) & 1 \end{bmatrix} \begin{bmatrix} 1 & -t_i(z^{-1}) \\ 0 & 1 \end{bmatrix} \begin{bmatrix} 1/K & 0 \\ 0 & K \end{bmatrix} \end{array} \right. \\ \left\{ \begin{array}{l} P(z) = \begin{bmatrix} K_1 & 0 \\ 0 & K_2 \end{bmatrix} \prod_{i=1}^m \begin{bmatrix} 1 & S_i(z) \\ 0 & 1 \end{bmatrix} \begin{bmatrix} 1 & 0 \\ t_i(z) & 1 \end{bmatrix} \\ \tilde{P}(z) = \begin{bmatrix} K_1 & 0 \\ 0 & K_2 \end{bmatrix} \prod_{i=1}^m \begin{bmatrix} 1 & \tilde{S}_i(z) \\ 0 & 1 \end{bmatrix} \begin{bmatrix} 1 & 0 \\ \tilde{t}_i(z) & 1 \end{bmatrix} \end{array} \right. \end{array} \right. \quad (2)$$

where  $P(z)$  is the reconstruction poly-phase matrix that rebuilds the original signal from its lifting scheme.  $S(z)$  and  $t(z)$  are Laurent polynomials that stand for prime lifting (update) and dual lifting (predict) steps, respectively.

The extracted coefficients (i.e.,  $t_i(z)$ ,  $S_i(z)$ ) from each of the common structures in Equation (2) should be applied to their respective lifting block diagrams (Figure 2a,b).

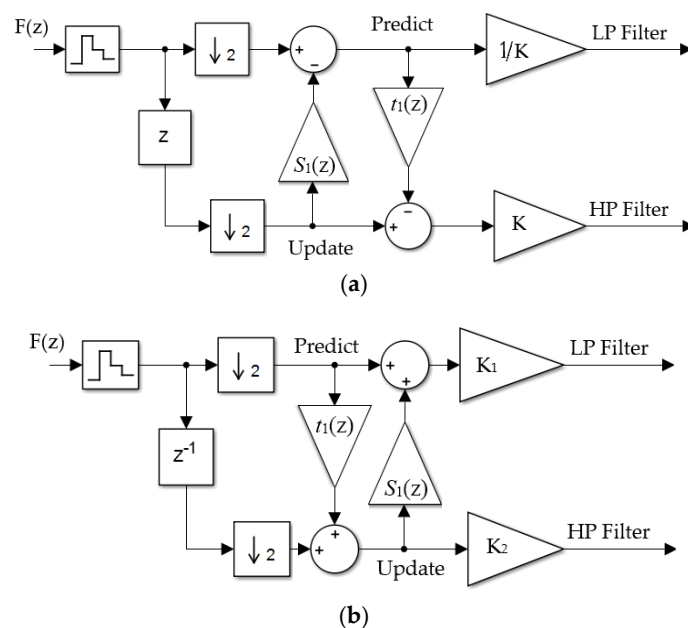


**Figure 2.** Schematics of lifting wavelet based on: (a) the first general structure; and (b) the second general structure.

### 2.1.2. Lifting Scheme-Based Low-Pass Filter

A wavelet-based low-pass filter is employed here instead of the conventional low-pass filters to extract the positive sequence component of power signal. This positive power extraction is needed for two reasons. First, is to implement the A-GTIP compensation algorithm to accurately control the AUPQS system. Second, the positive sequence component of the generated PV power is extracted to be injected into grid lines. A wavelet-based low-pass filter, instead of the conventional low-pass filters

within the A-GTIP control algorithm, highly improves the accuracy of the AUPQS. In [2], the A-GTIP compensation theory was proposed for controlling of active filters as follows:

$$\begin{cases} I_{P1}^+(t) = \frac{\overline{P_1^+}(t)}{\overline{V_S^+}(t) \cdot \overline{V_S^+}(t)} V_S^+(t) \\ I_C(t) = I_S(t) - I_{P1}^+(t) \end{cases} \quad (3)$$

This suggestion leads to overcoming the inaccuracy of the available compensation algorithms under asymmetric and distorted three-phase load-terminal voltages. Nonetheless, the employed conventional low-pass filter, used to extract  $P_1^+(t)$  within the A-GTIP algorithm (Equation (3)), shows a prolonged transient response particularly in the presence of grid-end low-order harmonics. Therefore, a wavelet-based low-pass filter with a lower response time, instead of conventional low-pass filters, is proposed to shorten and improve the transient response time of the AUPQS. The block diagram of the proposed LWT filter within the AUPQS controller is shown in Figure 3.

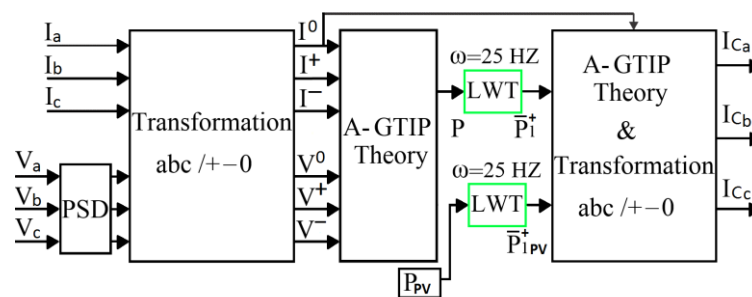


**Figure 3.** Block diagram of the advanced generalized theory of instantaneous power (A-GTIP) compensation algorithm equipped with wavelet-based filter.

Here the developed wavelet-based low-pass filter is also used to attenuate the injected PV power to the grid in a less transient response time.

## 2.2. The Damped Input Filter

### 2.2.1. The Design Principles and Criteria

Switching of the DC–DC converter injects numerous harmonics through the PV-end current and voltage waveforms. The Fourier series of the PV-end current demonstrates the presence of these injected harmonics as follows:

$$\begin{cases} i_{pv} = \frac{I}{(1-D)} + \sum \frac{2I}{k\pi} \sin(k\pi(1-D)) \cos(k\omega t) \\ i_{pv} = \frac{I \cdot H(0)}{(1-D)} + \sum || H(k \cdot j\omega) || \cdot \frac{2I}{k\pi} \sin(k\pi(1-D)) \cos(k\omega t) \end{cases} \quad (4)$$

where  $i_{pv}$  is the generated PV current, and  $I$  is the injected converter current into the power grid.  $D$  is the converter duty cycle. Thus, to suppress the harmonic components at the switching frequency, this paper employs an input filter. The proposed input filter (with transfer function of  $H(k \cdot j\omega)$ ) inserts high impedances in the frequencies equal to the PV-end harmonics (Equation (4) for  $H(k \cdot j\omega)$ ). In other words, the PV-end current harmonics are suppressed at all angular frequencies of  $k\omega$ . This results in a fast and smooth transient response of the PV's DC–DC converter. Nonetheless, the proposed input filter, if not designed well, deteriorates the stability of the PV system, inserting a pair of unstable poles into the PV system transfer function. Moreover, addition of the input filter leads the system output impedance becomes so large over wide frequency ranges that the PV power would be wasted into the input filter itself. Here, the extra element theorem is employed to analyze the effect of the inserted input filter into the PV system transfer function, since the extra element theorem is a useful tool to define the performance of a new inserted element within a system, as shown in Figure 4, with no need

to redefine all unwanted circuit elements which have already been obtained. This means a new transfer function will be derived for the DC–DC converter within the PV system, which is based on the previous system transfer function, estimating the effect of the input filter on the system performance. As shown in Equation (5), there is no need to algebraically redefine all of the PV unwanted elements [20].

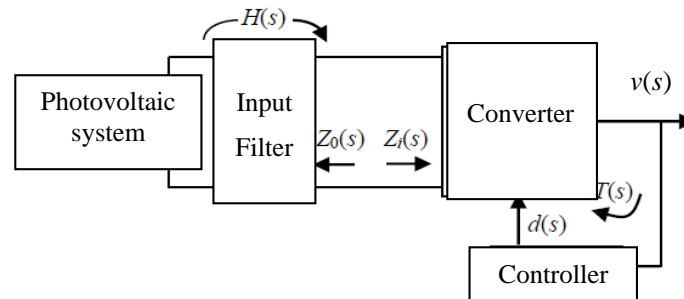


**Figure 4.** Schematic of the suggested input filter inserted between the PV system and DC (direct current)–DC converter.

If the control-to-output transfer function of the employed DC–DC converter is defined as  $G_{old} = v(s)/d(s)$  (Equation (5) for  $G_{old}$ ), addition of an input filter to the switching converter leads to the system illustrated in Figure 4. To determine the control-to-output transfer function in the presence of the input filter, it is assumed that  $V_{pv}$  (i.e., PV voltage-terminal voltage in Figure 4) equals zero. Thus, the input filter can be treated as an impedance (Figure 4 for  $Z_0(s)$ ). Further, based on the extra element theorem, the following equation can be extracted as:

$$\left\{ \begin{array}{l} G_{new}(s) = (G_{old}(s) \Big|_{z_0(s) \rightarrow 0}) \left( \frac{1 + \frac{Z_0(s)}{Z_N(s)}}{1 + \frac{Z_0(s)}{Z_D(s)}} \right) \\ \left\{ \begin{array}{l} \|Z_0(s)\| \leq \|Z_N(s)\| \\ \|Z_0(s)\| \leq \|Z_D(s)\| \end{array} \right. \end{array} \right. \quad (5)$$

where  $Z_D(s)$  equals  $Z_i(s)$ , when the feedback signal (i.e.,  $d(s)$ ) of the DC converter becomes zero (see Equation (6) for  $Z_D(s)$ ).  $Z_N(s)$  equals  $Z_i(s)$  when the duty cycle of the DC–DC converter ideally varies so that the small-signal voltage variation at load-terminal becomes zero. And  $Z_0(s)$  represents the input filter's impedance while the PV-end voltage is shortened. The parameters of  $Z_D(s)$ ,  $Z_N(s)$ , and  $Z_0(s)$  are calculated as follows [20]:

$$\left\{ \begin{array}{l} Z_D(s) = (D^2 R) \cdot \frac{[1 + \frac{sL}{D^2 R} + s^2 \frac{LC}{D^2}]}{(1 + sRC)} \\ Z_N(s) = -D^2 R \cdot (1 - \frac{sL}{D^2 R}) \\ Z_0(s) = LS \parallel \frac{1}{CS} \end{array} \right. \quad (6)$$

$Z_0(s)$  in Equation (6) also indicates the filter resonant frequency, where the inductor and capacitor are intersected. Since the filter is un-damped ( $R = 0$ ), the input filter does not satisfy the stability requirements of the new derived transfer function (substitute Equation (6) into Equation (5)). The solution is to include a resistance along with either capacitance or inductance within the input filter; then, it leads to have a damped input filter. However, the dissipated power by this inserted impedance can sometimes be even more than the system's load itself. Hence, optimum structures should be investigated [20,21]. Under an optimum structure satisfying Equation (5), the inserted input filter consequently does not substantially change the magnitude of the new transfer function; because, the correction factor's gain within Equation (5) remains at unity. With these considerations, the designed input filter removes transients and disturbances of the PV system at the entrance of the DC–DC converter.

### 2.2.2. Optimal Design of the Damped Input Filter

The boost converter, like other switch converters, does not include time-invariant linear circuits. Thus, to control output transfer function of the boost converter, its small-signal linear model must be developed. Accordingly, extracting  $Z_N$  and  $Z_D$  (Equation (6)), and solving an optimization problem, the maximum allowable value for  $Z_0$  is estimated with regard to the value of  $n$  (Equation (7) for  $Z_0$ ). Several practical approaches are to damp the proposed input filter. Here, a parallel damping approach is used [20]. In this method, a damping resistor (i.e.,  $R_f$ ) in series with an inductance ( $L_{dp}$ ) are placed in parallel with the input filter's inductance (Figure 5 for  $L_1$  and  $L_2$ ). Inductor  $L_{dp}$  causes the filter to exhibit a two-pole characteristics at high frequencies. However, the  $L_{dp}$  should include a much smaller impedance value at the resonance frequency. This allows the  $R_f$  to dampen the input filter.  $\|Z_0(j\omega)\|$  for a given  $L_{dp}$  is calculated by the following equations:

$$\left\{ \begin{array}{l} \left\{ \begin{array}{l} Q_{opt1} = \frac{R_{f1}}{R_{filter1}} = \sqrt{\frac{n(3+4n)(1+2n)}{2(1+4n)}} \\ \|Z_0(j\omega)\| = R_{filter1} \sqrt{2n(1+2n)} \end{array} \right. \\ \left\{ \begin{array}{l} L_1 = \frac{R_{filter1}}{2\pi F_{f1}} \\ C_1 = \frac{1}{2\pi F_{f1} R_{filter1}} \\ n_1 = n_2 = n = \frac{L_{dp1}}{L_1} = \frac{L_{dp2}}{L_2} (s) \end{array} \right. \end{array} \right. \quad (7)$$

where  $Q_{opt1}$  is the optimum  $Q$ -factor of the designed filter,  $R_{f1}$  represents the damping resistance,  $R_{filter1}$  is the original characteristic impedance (which equals to  $R_{filter1} = \sqrt{L_1/C_1}$ ),  $\|Z_0(j\omega)\|$  introduces the optimum peak value of the output impedance of the designed input filter, and  $L_{dp}$  stands for the inductance of the parallel damping branch, as shown in Figure 5.  $n$  is equal to  $L_{dp1}/L_1$ .  $F_{f1}$  presents the input filter cut-off frequency of Section 1, and should be smaller than the cut off frequency of Section 2 (i.e.,  $F_{f1} < F_{f2}$ ). As a result, the attenuation of Section 1 would be much greater than Section 2. For a cascaded input filter, this design procedure would be repeated to determine the optimum element values for each cascade section (Figure 5, for  $L_1$ ,  $C_1$ ,  $L_2$ , and so on.) The optimization's goal is to minimize passive element values within the input filter.

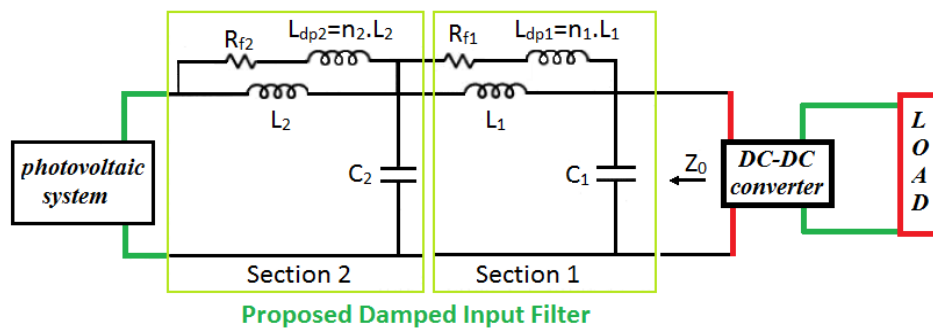
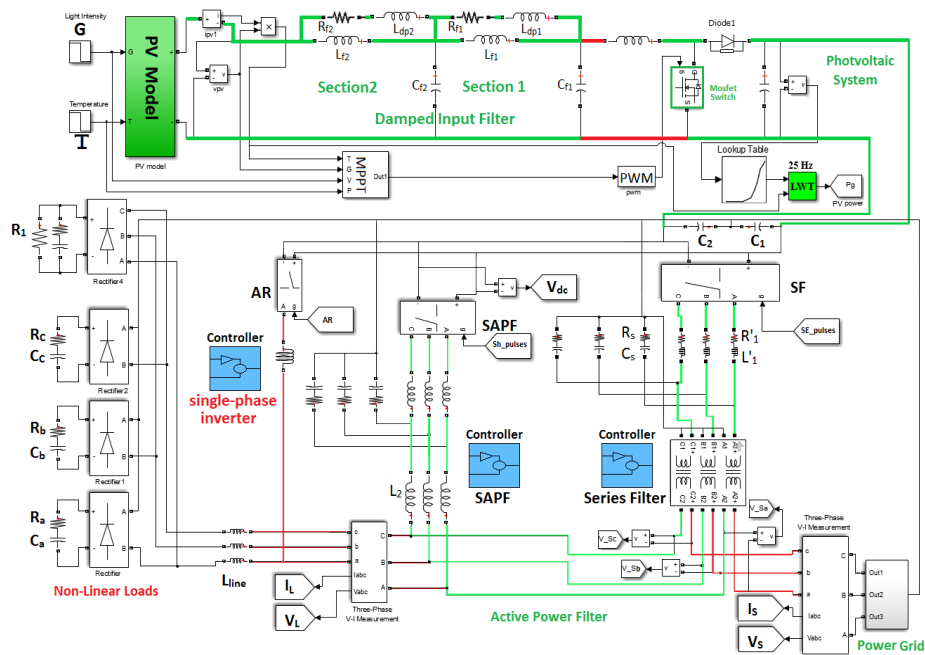


Figure 5. Suggested cascading input filter within the DC-DC converter of the PV system.

### 3. Simulations and Discussion

To verify the effectiveness of both the proposed wavelet-based low-pass filter and the input filter, an integrated PV system-to-power grid using an active filter is simulated, as shown in Figure 6. This integrated system consists of PV arrays, an MPPT system, input filter, the DC-DC boost converter, and unbalanced non-linear capacitive loads, as well as the active filter (the AUPQS). The non-linear capacitive loads consist of three single-phase rectifiers plus a three-phase rectified load. Table 1 presents the parameters of the non-linear loads.



**Figure 6.** Simulation of proposed damped input filter within a grid-integrated PV system via an active filter.

**Table 1.** Parameters of single-phase and three-phase loads in Figure 6.

Parameters	$R_a$	$C_a$	$R_b$	$C_b$	$R_c$	$C_c$	$R_1$	$R_2$	$C_2$
Unit	$\Omega$	mF	$\Omega$	mF	$\Omega$	mF	$\Omega$	$\Omega$	mF
Value	0.5	0.5	0.33	50	0.33	5.0	3.0	0.5	50

The inverter parameters of the AUPQS and its designed LCL filter are listed in Table 2. Table 3 presents the parameters of the proposed cascaded input filter (Figure 6).

**Table 2.** Parameters of the advanced universal power quality conditioning system (AUPQS).

Parameters	Value	Unit
AR inductance $L_{AR}$	1	mH
Inductance $L'_1$	0.6	mH
Resistance $R'_1$	30	m $\Omega$
LCL filter capacitor $C_s$	220	$\mu$ F
LCL filter damping resistor $R_s$	0.5	$\Omega$
SAPF LCL filter inductance $L_1$	4.1	mH
Grid side LCL filter inductance $L_2$	0.5	mH
LCL filter capacitor $C_f$	10	$\mu$ F
LCL filter damping resistor $R_f$	20	$\Omega$
SAPF Switching frequency	6.9	kHz
SAPF DC-link capacitor	2	mF
SAPF DC-link voltage	850	V

**Table 3.** Optimum element values of cascading input filter in Figure 6.

Parameters	$R_{f1}$	$L_{dp1}$	$L_{f1}$	$C_{f1}$	$R_{f2}$	$L_{dp2}$	$L_{f2}$	$C_{f2}$
Unit	$\Omega$	$\mu$ H	$\mu$ H	$\mu$ H	$\mu$ H	$\mu$ H	$\mu$ H	$\mu$ H
Value	35	238	476	0.32	9.7	43.9	87.8	0.78

It is assumed that the PV system is able to regulate the DC link and injecting power to the AC loads; however, whenever the DC link regulation needs more power, using a lookup table, the injection level of the PV power to the grid lines decreases to 80%, 60%, 40%, or even 20% of its value, respectively. Table 4 presents one module profile of the PV system.

**Table 4.** One solar module profile (at 25 °C and 1000 W/m<sup>2</sup>).

Parameters	$P_{max,m}$	$I_{sc,n}$	$V_{oc,n}$	$K_V$	$K_I$	$T_n$	$G_n$
Unit	W	A	V	V/K	A/K	°C	W/m <sup>2</sup>
Value	200.143	8.21	32.9	−0.123	0.032	25	1000

The MPPT system involves a hybrid algorithm with two control loops, namely a set-point calculation loop and a fine tuning loop. The set-point calculation loop estimates the solar arrays maximum power at the startup time as well as under sudden environmental changes such as ambient solar cell temperature variations.

For this reason, the maximum open circuit voltage of the PV system is initially extracted using the following solar cell short-circuit current ( $I_{sc}$ ) and open-circuit voltage ( $V_{oc}$ ).

$$\left\{ \begin{array}{l} \left\{ \begin{array}{l} I_{sc} = I_{sc,n}(\frac{G}{G_n}) + K_I(T - T_n) \\ V_{oc} = V_{oc,n} + K_V(T - T_n) - (I_{sc} - I_{sc,n})R_S \end{array} \right. \\ V_{oc} = V_{oc,n} + (K_V - R_S K_I) \times (T - T_n) - ((\frac{G}{G_n}) - 1)I_{sc,n}R_S \\ V_{MPP} = KV_{oc} \end{array} \right. \quad (8)$$

where  $I_{sc,n}$  and  $V_{oc,n}$  are the solar short-circuit current and open-circuit voltage at the standard conditions (i.e., a temperature equal to 25 °C ( $T_n$ ) and light intensity ( $G_n$ ) equal to 1000 W/m<sup>2</sup>), respectively. The  $K_V$  and  $K_I$  coefficients are provided by the manufacturer at the solar panel data sheet.

The open-circuit voltage ( $V_{oc}$ ) can be defined by measuring instant solar cell temperature ( $T$ ) and light intensity ( $G$ ) variations. Hence,  $V_{oc}$  can be determined, unlike the offline MPPT algorithms, without the need of load shedding. Now, the  $V_{MPP}$  can be estimated as a fraction ( $K$ ) of the measured  $V_{oc}$  (i.e., Equation (8) for  $V_{MPP}$ ). The initial value for the  $K$  is usually assumed to be between 0.8 and 0.9. To obtain an accurate value for the  $K$ , the proposed MPPT algorithm suggests one of the online MPPT approaches, such as the P and O method, to find an accurate  $K$ . The online MPPT algorithm estimates the precise value of the  $K$  via either adding or subtracting a constant  $\Delta K$  from the assumed  $K$  (i.e.,  $K_{new} = K + \Delta K$ ) to estimate exact value of  $V_{MPP}$  (i.e.,  $V_{MPP} = KV_{oc}$ ). This means that the measured maximum open-circuit voltage for the presumed  $K + \Delta K$  ( $K - \Delta K$ ) is repeatedly compared with the PV-terminal voltage. Then, the direction of the PV power changes in each turn defines the direction of the next  $\Delta K$  (i.e., to be positive or negative); subsequently, the generated signal error is applied to a proportional integrator (PI) controller to adjust the duty cycle of the DC–DC converter (Equation (9)).

$$\left\{ \begin{array}{l} \left\{ \begin{array}{l} \frac{V_L}{V_{pv}} = \frac{1}{1-D} \\ \rightarrow V_{pv} = (1 - D)V_L \end{array} \right. \\ \text{if : } V_{pv} = V_{MPP} \rightarrow D = D_{MPP} \end{array} \right. \quad (9)$$

The generated signal error is applied to a pulse with modulation (PWM) signal generator to produce the optimum duty cycle for the MOSFET within the DC–DC converter. Then, the MOSFET switching, as shown in Figure 6, forces the PV system to operate on its maximum power point [1].

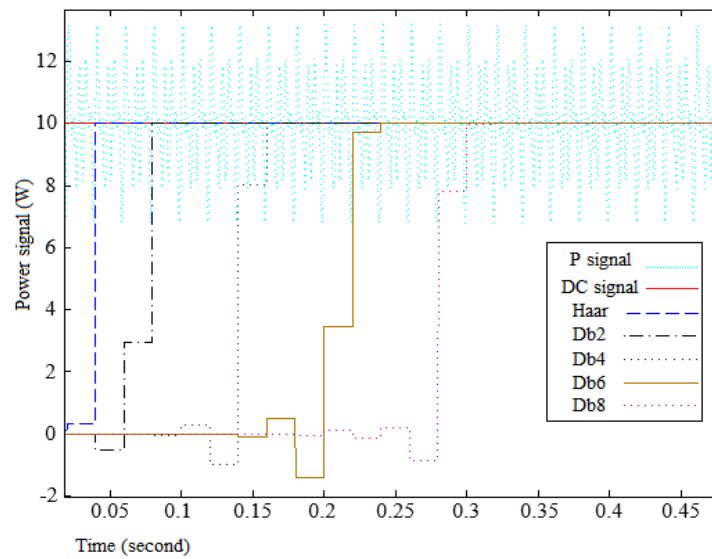
### 3.1. Wavelet-Based Low-Pass Filter

The employed mother wavelet and the lowest bandpass frequency are very important factors to design a wavelet-based low-pass filter [30].

### 3.1.1. Mother Wavelet

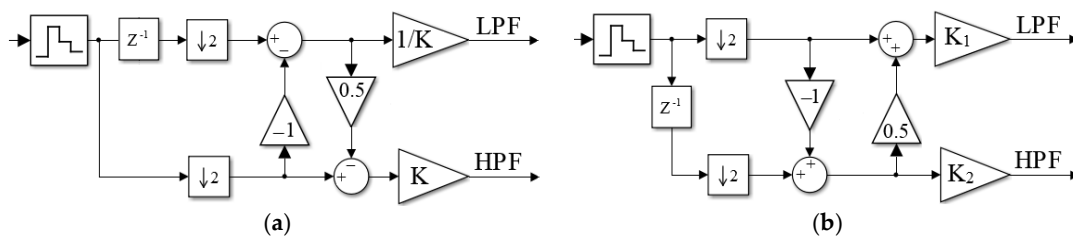
Here, to evaluate the accuracy of the chosen mother wavelet for the designed wavelet-based filter, five popular mother wavelets such as Haar, daubechie 2 (db2), daubechie 4 (db4), daubechie 6 (db6), and daubechie 8 (db8) are examined as shown in Figure 7. The original power signal contains a DC signal plus second-, third-, and fifth-order harmonics (Figure 7 for  $P_{\text{signal}}$ ).

Figure 7 shows that the more complicated the mother wavelet, the larger the filter’s transient time become. The Haar mother wavelet with a flat bandpass characteristic shows the shortest raised time. This means the Haar wavelet-based low-pass filter can properly extract the DC component of a power signal which includes periodical harmonics.



**Figure 7.** The extracted DC signals using a wavelet-based low-pass filter controlled by different mother wavelets.

The lifting-based wavelet theory simply estimates the Haar mother wavelet coefficients (namely approximation low pass filter (LPF) and detail high pass filter (HPF) coefficients), as shown in Figure 8. In this research, the Haar mother wavelet is employed to control the proposed wavelet-based filter.



**Figure 8.** Simulated block diagrams for the Haar mother wavelet based on: (a) first general lifting-scheme; and (b) second lifting-scheme (Section 2).

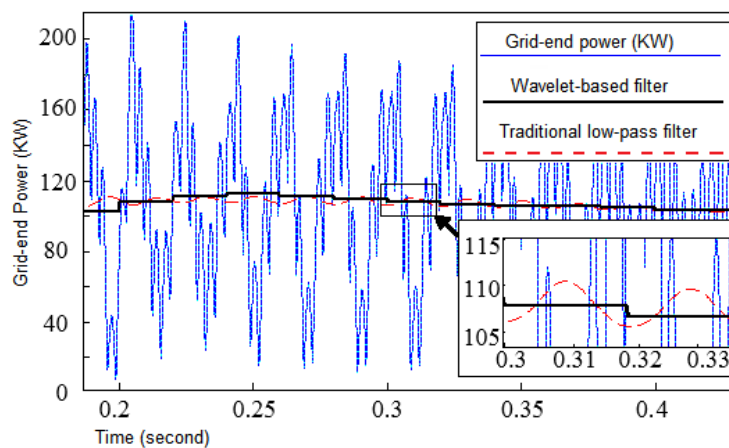
### 3.1.2. Lowest Bandpass Frequency

If  $f_u$  indicates the lowest frequency range which only contains the DC component of the original signal, and  $f_s$  represents the signal sampling rate, then the needed lifting blocks to extract the DC signal are defined as follows [31]:

$$f_u \times 2 = \frac{f_s}{2^n} \tag{10}$$

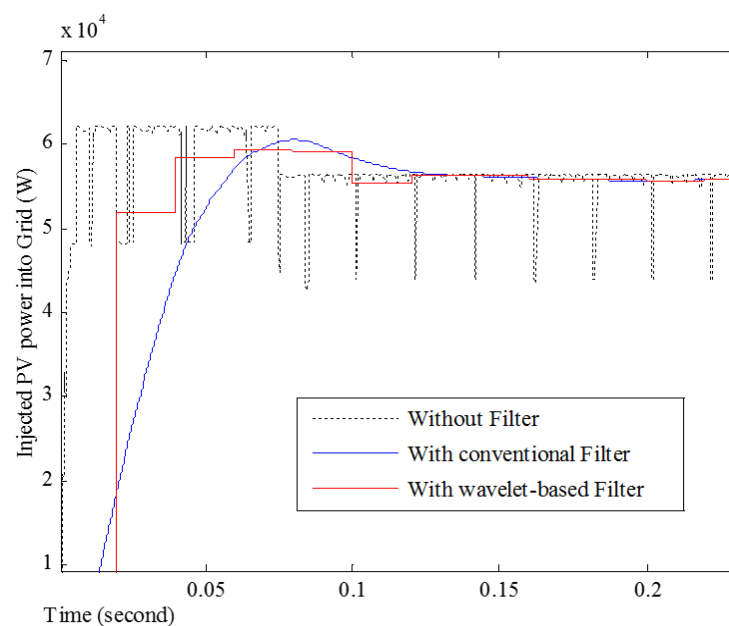
In this research, the sampling rate is selected as 1600 Hz, and the upper limit of 25 Hz is assumed for the filter lowest band to extract the DC signal. Thus, the wavelet-based filter includes five lifting blocks to extract the DC component of the original signal.

Figure 9 shows that the proposed wavelet-based filter within the AUPQS controller accurately extracts the positive sequence component of the grid-end active power in less transient response time. The conventional low-pass filter, on the contrary, results in the extracted positive sequence component of active power after 30 ms still oscillates around its DC value, as can be seen in Figure 9.



**Figure 9.** Positive component of grid-end active power extracted by the proposed wavelet-based low-pass filter and the conventional low-pass filter.

Figure 10 compares the rising time of the injected PV power to the grid lines when the wavelet-based and the conventional low-pass filter are employed. The proposed wavelet-based low-pass filter with a less transient response time accurately extracts the positive sequence component of the PV power, as shown in Figure 10.



**Figure 10.** Extracted positive component of the injected PV power to the grid, using the wavelet-based low-pass filter and conventional low-pass filter. The sun irradiation decreases at 0.075 s from  $1000 \text{ W/m}^2$  to  $900 \text{ W/m}^2$ .

### 3.2. Optimum Damped Input Filter

In this section, accuracy of the proposed damped input filter is evaluated under two conditions. First, when the PV system meets a constant DC load at its boost converter's terminal; and secondly, the PV system is interfaced with the power system via the AUPQS. In this case, the PV system applies the generated power to firstly supply the DC link of the AUPQS, and then the excess positive sequence of the generated power is injected through the grid lines via the AUPQS inverters.

Figure 11 demonstrates that the proposed input filter highly suppresses distortions during the PV startup time condition, when the generated PV power is used to supply a time-invariant resistive load ( $R = 100 \Omega$ ). The light intensity is assumed as  $1200 \text{ W/m}^2$  and the ambient cell temperature is set to  $25 \text{ }^\circ\text{C}$ . Figure 12 shows that the suggested damped input filter works accurately to improve the transient response of the PV system under time-variant load conditions. In this case, the PV output power supplies the DC link of the AUPQS. A sudden light intensity variation from  $1000 \text{ W/m}^2$  to  $1200 \text{ W/m}^2$  is assumed at  $0.075 \text{ s}$ .

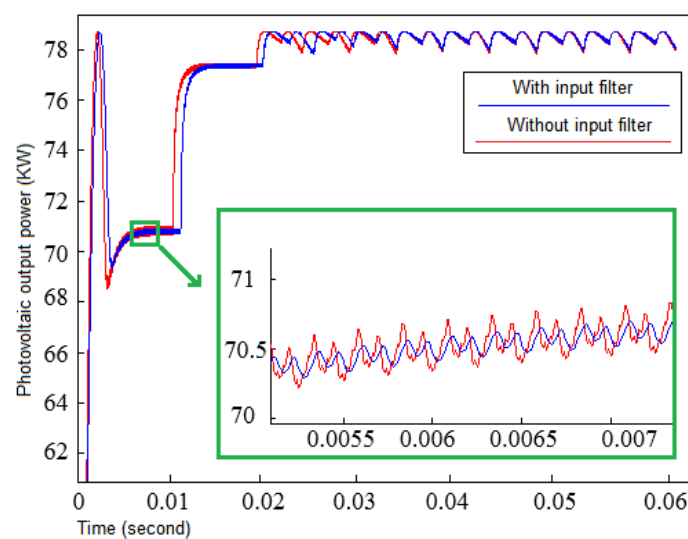


**Figure 11.** The generated PV power under a transient startup condition with/without the designed damped input filter.

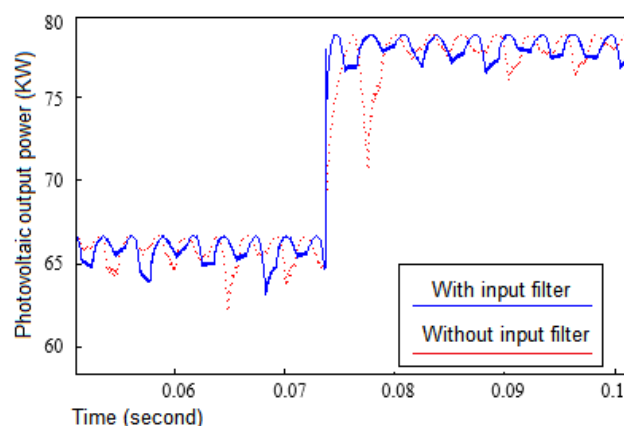


**Figure 12.** The generated PV power under a nonlinear time-variant load while a sudden light intensity variation ( $1000\text{--}1200 \text{ W/m}^2$ ) occurs at  $0.075 \text{ s}$ .

Figure 13 demonstrates the AC grid-end currents under sun irradiation variation from  $1000 \text{ W/m}^2$  to  $750 \text{ W/m}^2$  at  $0.025 \text{ s}$ . Equipped with the wavelet-based low-pass filter and the proposed input

filter, the integrated power system, in an accurate transient time, increases the currents accordingly to provide the load with enough power (see Figure 13 for the AC grid-end current at 0.025 s). On the contrary, the conventional active filter after 0.5 s can supply the load demand. This means that the delay of the active filter, due to the prolonged operation of its conventional low-pass filter along with a lack of a proposed input filter, can highly prolong the transient response of the grid-connected PV system.

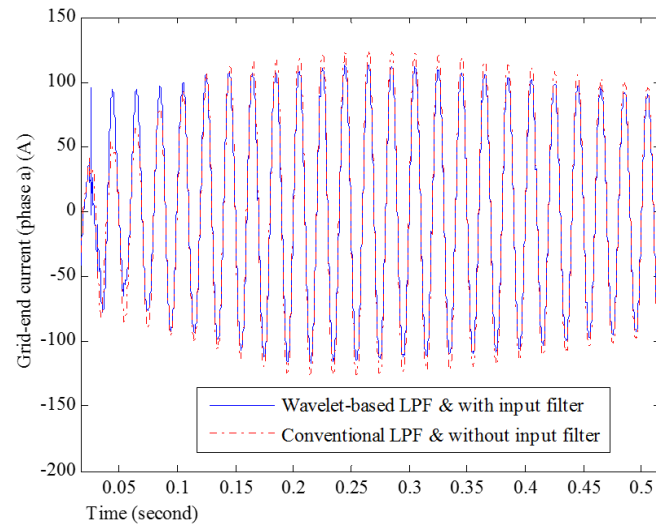


**Figure 13.** Comparison of transient response time of compensated grid-end current (Phase A) by the conventional low-pass filter and by the proposed wavelet-based low-pass filter, together with the suggested input filter under sun irradiation variation from  $1000 \text{ W/m}^2$  to  $750 \text{ W/m}^2$  at 0.025 s.

#### 4. Conclusions

A wavelet-based low-pass filter is developed and compared with the conventional low-pass filter through the AUPQS control algorithm. To further reduce the transient response time of an integrated PV unit-to-power system, the designed wavelet-based filter is also applied to extract the positive sequence of the generated PV power, injected to the grid lines. Suppressing the PV-end power distortions and harmonics, this paper also suggests the application of the damped input filter within the PV's DC–DC converter. This suggestion results in the PV DC–DC converter's switching being damped in an accurate transient time. This also leads the available MPPT controllers to work with much more stability and precision. Simulation results verify that the proposed wavelet-based low-pass filter, together with the suggested input filter, lead an integrated power system to enjoy a reduced transient response time, fully compensating the grid-end current distortions (see Figure 13 for the grid-end current).

**Acknowledgments:** This work has been supported by China Government Scholarship and the Fundamental Research Funds for the Central Universities (HIT.NSRIF.201143).

**Author Contributions:** Weixing Li conceived and designed the simulations; Bijan Rahmani performed the simulations; Weixing Li and Bijan Rahmani analyzed the data; Bijan Rahmani wrote the paper.

**Conflicts of Interest:** The authors declare no conflict of interest.

#### Abbreviations

AUPQS	Advanced universal power quality conditioning system
A-GTIP	Advanced generalized theory of instantaneous power
AR	Active rectifier
FIR	Finite impulse response
LWT	Lifting scheme-based wavelet filter

PV	Photovoltaic system
SAPF	Shunt active power filter
SF	Series active filter
$I_L$	Load-end currents
$I_{PV}$	PV-end current
$I_S$	Source-end currents
$P_{PV}$	Photovoltaic output power
$V_L$	Load-terminal voltages
$V_S$	Source voltages
$V_S^+$	Positive component of grid voltages

## References

1. Rahmani, B.; Li, W.; Liu, G. An advanced universal power quality conditioning system and MPPT method for grid integration of photovoltaic systems. *Int. J. Electr. Power Energy Syst.* **2015**, *69*, 76–84. [[CrossRef](#)]
2. Rahmani, B.; Bina, M.T. Reciprocal effects of the distorted wind turbine source and the shunt active power filter: Full compensation of unbalance and harmonics under “capacitive non-linear load” condition. *IET Power Electron.* **2013**, *6*, 1668–1682. [[CrossRef](#)]
3. Depenbrock, M.; Staudt, V.; Wrede, H. Concerning “instantaneous power compensation in three-phase systems by using p–q–r theory”. *IEEE Trans. Power Electron.* **2004**, *19*, 1151–1152. [[CrossRef](#)]
4. Modarresi, J.; Bina, M.T.; Golkar, M.A. Improving the p-q compensation method in the presence of low-order harmonics by LWT: Theory and implementation. *Int. Rev. Electr. Eng.* **2012**, *7*, 5022–5028.
5. Modarresi, J.; Fallah, M.; Gholipour, E.; Bina, M.T. Improving the SRF method to compensate low-order harmonics under nonsinusoidal network voltages. *Turk. J. Electr. Eng. Comput. Sci.* **2016**, *24*, 412–426. [[CrossRef](#)]
6. Tse, N.C.F.; Chan, J.Y.C.; Lau, W.H.; Poon, J.T.Y.; Lai, L.L. Real-time power-quality monitoring with hybrid sinusoidal and lifting wavelet compression algorithm. *IEEE Trans. Power Deliv.* **2012**, *27*, 1718–1726. [[CrossRef](#)]
7. Chen, C.-L.; Xu, T.Y.; Yuan, Y.; Jiang, F. Detection and Location of Power Quality Transient Disturbance Based on Lifting Wavelet. In Proceedings of the 2010 Asia-Pacific Power and Energy Engineering Conference, Chengdu, China, 28–31 March 2010; pp. 1–4.
8. Wang, Z.; Bian, S.; Lei, M.; Zhao, C.; Liu, Y.; Zhao, Z. Feature extraction and classification of load dynamic characteristics based on lifting wavelet packet transform in power system load modeling. *Int. J. Electr. Power Energy Syst.* **2014**, *62*, 353–363. [[CrossRef](#)]
9. Nwobu, C.J.; Zhang, L. Lifting Wavelet Transform and Energy Operator Synchronization for a Flying Capacitor Multi-Level Inverter Based Active Power Filter. In Proceedings of the 2013 15th European Conference on Power Electronics & Applications (EPE), Lille, France, 2–6 September 2013; pp. 1–10.
10. Yilmaz, A.S.; Subasi, A.; Bayrak, M.; Karsli, V.M.; Ercelebi, E. Application of lifting based wavelet transforms to characterize power quality events. *Energy Convers. Manag.* **2007**, *48*, 112–123. [[CrossRef](#)]
11. Noguchi, T.; Togashi, S.; Nakamoto, R. Short-current pulse-based maximum power-point tracking method for multiple photovoltaic and converter module system. *IEEE Trans. Ind. Electron.* **2002**, *49*, 217–223. [[CrossRef](#)]
12. Eram, T.; Chapman, P.L. Comparison of photovoltaic array maximum power point tracking techniques. *IEEE Trans. Energy Convers.* **2007**, *22*, 439–449. [[CrossRef](#)]
13. Subudhi, B.; Pradhan, R. A comparative study on maximum power point tracking techniques for photovoltaic power systems. *IEEE Trans. Sustain. Energy* **2012**, *4*, 89–98. [[CrossRef](#)]
14. Cheng, P.; Peng, B.; Liu, Y.; Cheng, Y.; Huang, J. Optimization of a fuzzy-logic-control-based MPPT algorithm using the particle swarm optimization technique. *Energies* **2015**, *8*, 5338–5360. [[CrossRef](#)]
15. Li, C.; Chen, Y.; Zhou, D.; Liu, J.; Zeng, J. A high-performance adaptive incremental conductance MPPT algorithm for photovoltaic systems. *Energies* **2016**, *9*, 288. [[CrossRef](#)]
16. Wang, M.; Huang, M.; Jiang, W. Maximum power point tracking and harmonic reducing control method for generator-based exercise equipment. *Energies* **2016**, *9*, 103. [[CrossRef](#)]
17. Tsai, C.; Chen, W. Buck converter with soft-switching cells for PV panel applications. *Energies* **2016**, *9*, 148. [[CrossRef](#)]

18. Chen, Y.M.; Liu, Y.C.; Wu, F.Y. Multiinput converter with power factor correction, maximum power point tracking, and ripple-free input currents. *IEEE Trans. Power Electron.* **2004**, *19*, 631–639. [[CrossRef](#)]
19. Sait, H.H.; Daniel, S.A. New control paradigm for integration of photovoltaic energy sources with utility network. *Int. J. Electr. Power Energy Syst.* **2011**, *33*, 86–93. [[CrossRef](#)]
20. Erickson, R.W.; Maksimovic, D. *Fundamental of Power Electronics*, 2nd ed.; Springer US: New York, NY, USA, 2001; pp. 385–404.
21. Erickson, R.W. Optimal single resistors damping of input filters. In Proceedings of the 1999 IEEE Applied Power Electronics Conference and Exposition, Dallas, TX, USA, 14–18 March 1999; pp. 1073–1097.
22. Spiazzi, G.; Pomilio, J.A. Interaction between EMI filter and power factor preregulators with average current control: Analysis and design considerations. *IEEE Trans. Ind. Electron.* **1999**, *46*, 577–584. [[CrossRef](#)]
23. Jang, Y.; Erickson, R.W. Physical origins of input filter oscillations in current programmed converters. *IEEE Trans. Power Electron.* **1992**, *7*, 725–733. [[CrossRef](#)]
24. Erich, S.; Polivka, W.M. Input filter design for current-programmed regulators. In Proceedings of the 1990 IEEE Applied Power Electronics Conference and Exposition, Los Angeles, CA, USA, 11–16 March 1990; pp. 781–791.
25. Anzalchi, A.; Moghaddami, M.; Moghaddasi, A.; Sarwat, A.; Rathore, A. A new topology of higher order power filter for single-phase grid-tied voltage source inverters. *IEEE Trans. Ind. Electron.* **2016**, *99*. [[CrossRef](#)]
26. Channegowda, P.; John, V. Filter optimization for grid interactive voltage source inverters. *IEEE Trans. Ind. Electron.* **2010**, *57*, 4106–4114. [[CrossRef](#)]
27. Wu, W.; He, Y.; Blaabjerg, F. An LLCL power filter for single-phase grid-tied inverter. *IEEE Trans. Power Electron.* **2012**, *27*, 782–789. [[CrossRef](#)]
28. Ray, P.K.; Kishor, N.; Mohanty, S.R. Islanding and power quality disturbance detection in grid-connected hybrid power system using wavelet and s-transform. *IEEE Trans. Smart Grid* **2012**, *3*, 1082–1094. [[CrossRef](#)]
29. Lave, M.; Kleissl, J.; Stein, J.S. A wavelet-based variability model (WVM) for solar PV power plants. *IEEE Trans. Sustain. Energy* **2013**, *4*, 501–509. [[CrossRef](#)]
30. Pigazo, A.; Liserre, M.; Mastromauro, R.A.; Moreno, V.M.; Dell’Aquila, A. Wavelet-based islanding detection in grid-connected PV systems. *IEEE Trans. Ind. Electron.* **2009**, *56*, 4445–4455. [[CrossRef](#)]
31. Forghani, M.; Afsharnia, S. Online wavelet transform-based control strategy for UPQC control system. *IEEE Trans. Power Deliv.* **2007**, *22*, 481–491. [[CrossRef](#)]



© 2016 by the authors; licensee MDPI, Basel, Switzerland. This article is an open access article distributed under the terms and conditions of the Creative Commons Attribution (CC-BY) license (<http://creativecommons.org/licenses/by/4.0/>).